Nanoparticle Scanners for the Identification of Key Sequences Involved in the Assembly and Disassembly of *β*-Amyloid Peptides

*Milad Zangiabadi, Avijit Ghosh, and Yan Zhao**

Department of Chemistry, Iowa State University, Ames, Iowa 50011-3111, U.S.A.

zhaoy@iastate.edu

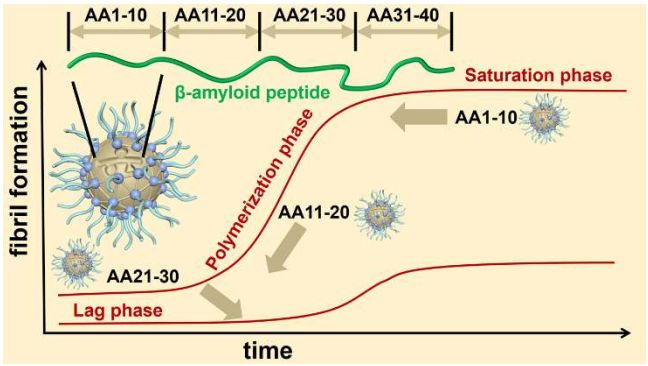

ABSTRACT. Aggregation of β-amyloid peptides (Aβ), implied in the development and progression of Alzheimer's disease, is driven by a complex set of intramolecular and intermolecular interactions involving both hydrophobic and polar residues. The key residues responsible for the forward, assembling process may be different from those that should be targeted to disassemble already formed aggregates. Molecularly imprinted nanoparticle (MINP) receptors are reported in this work to bind specific segments of $A\beta_{40}$ strongly and selectively. Combined fluorescence spectroscopy, atomic force microscopy (AFM) imaging, and circular dichroism (CD) spectroscopy indicate that binding residues 21–30 near the loop region is the most effective to inhibit the aggregation of monomeric $A\beta_{40}$, but residues 11–20 that include

the internal β strand closer to the N terminal represent the best target for disaggregating already formed aggregates in the polymerization phase. Once the aggregation proceeds to the saturation phase, binding residues 1–10 has the largest effect on the disaggregation, likely due to accessibility of these amino acids relative to others to the MINP receptors.

Keywords: amyloid peptide; fibrillation; aggregation; self-assembly; disaggregation; molecular imprinting; binding

Introduction

Protein misfolding exposes aggregation-prone sequences and triggers their self-assembly into amyloid fibrils and ultimately plaques associated with Alzheimer's disease (AD), Parkinson's disease (PD), Type-II diabetes, and dozens of other pathological states.[1,2] The amyloid cascade hypothesis considers β-amyloid peptides (Aβ) key causative agents of AD and their aggregation associated with the development and progression of the disease.[3] These peptides are cleaved from amyloid precursor proteins and contain approximately 39–42 amino acid (AA) residues. Their aggregation happens in three stages (Figure 1):[2] a lag phase involving initial aggregation of the monomers into soluble, toxic oligomers,[4,5] a polymerization phase that converts the monomers and oligomers into larger aggregates, and a saturation phase in which protofilaments mature into more stable but less toxic amyloid fibrils.[2]

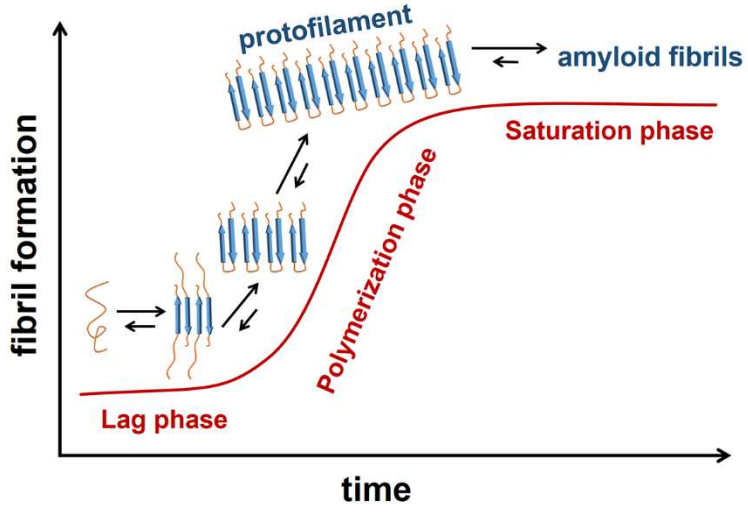

Figure 1. Aggregation of Aβ over different stages of aggregation to from fibrils.

Both experimental and computational modeling indicate that hydrophobic residues 17–21 (LVFFA) and 31–36 (IIGLMV) in Aβ are strong contributors to the aggregation.[6-9] Hydrogen-bonding and hydrophobic contact among these residues are key to the folding of the peptide into a U-turned β-sheet and further, intermolecular aggregation of the sheets into fibrils.[2] An intramolecular salt bridge between D23 and K28 is required to stabilize the turn structure, according to both solid-state NMR spectroscopy[6] and molecular simulations.[9] Other interactions also contribute to the aggregation, such as salt bridges between K16 & E22 among neighboring amyloid filaments as revealed by NMR spectroscopy [6] and cryo-EM.[10]

For a long peptide such as Aβ, therefore, a complex set of noncovalent interactions drive both the conformational change of the peptide and its aggregation into different self-assembled structures in a time-dependent manner. To control the assembly and disassembly at different stages, it is crucial to identify the "hot sequences" involved not only in the forward, aggregation process but also those in the backward reaction. These hot sequences most likely are different for the forward and backward processes, because the most-aggregation-prone segments in the assembly should be buried inside the aggregates, and binding exposed residues on the surface of the aggregate may be more effective than those less accessible, already locked ones to dissemble the aggregates. Not only so, dynamics and accessibility of the exposed residues in loosely associated aggregates found in the early stage of the self-assembly likely are different from those on the more ordered Aβ fibrils formed in the later stage.[11] Identification of the most "disaggregation-triggering" sequence is important to control of the self-assembly process and potentially development of effective drugs for AD.[2,12]

Researchers in recent years continue to devote tremendous efforts to understand how different agents interact with Aβ, whether to guide the aggregation along more benign pathways for potential therapeutic effects[2,13-24] or enable diagnostic tools sensitive to specific states of the peptide.[25-28] However, co-aggregation with a long, complex peptide is a difficult-to-control process. Different agents may co-assemble with Aβ to form alternative aggregates, convert toxic oligomers into less toxic fibrils,[2] or disassemble oligomers into nontoxic low MW species, depending on how they interact with Aβ and at

what stage the interaction takes place.[29] Likewise, antibodies can also interact with Aβ in different ways to exert diverse effects on the self-assembling processes.[30,31] Antibodies against residues 4–10 of $A\beta_{42}$, for example, are found to inhibit fibrillization and disassemble preformed fibrils, but the blocking mechanism gives the possibility of producing more toxic oligomers.[32,33] Antibody 3D6 against AAs 1–5 delays fiber formation but does not seem to alter oligomerization.[34]

In this work, we report molecularly imprinted nanoparticles (MINPs) with predetermined binding selectivity and biologically competitive binding affinity for Aβ. These MINPs serve as "nanoscanners" to target different segments of $A\beta_{40}$. By studying how the binding affects the assembly/disassembly at different stages of aggregation, we identify the hot sequences of Aβ responsible for a particular process through a combination of fluorescence spectroscopy, AFM imaging, and CD spectroscopy. Our scanning reveals that binding residues 21–30 is the most effective in the inhibition of the aggregation of monomeric $A\beta_{40}$ but residues 11-20 represent the best target for disaggregating already formed aggregates during the polymerization phase. To disassemble fibrils formed in the saturation phase, binding residues 1–10 has the largest effects.

Results and Discussion

Synthesis and Characterization of MINPs. Molecular imprinting is a powerful technique to create tailor-made binding sites for a wide variety of molecules in a polymer matrix.[35-37] In this method, template molecules are polymerized and cross-linked in the presence of functional monomers (FMs) to bind the templates and large amounts of cross-linkers to capture the template–FM complex in the cross-linked polymer network. Removal of the templates vacates the imprinted binding sites, which are ideally complementary to the templates in size, shape, and distribution of functional groups.

Molecularly imprinted polymers (MIPs) have been generated for peptides[38-50] and also for amyloid peptides.[41] Nonetheless, most of these are macroscopic polymeric materials. In order to scan a peptide and identify the key residues responsible for a particular assembling or disassembling process, one needs to minimize the dimension of the polymeric receptor, to the point that a particular segment of a long

peptide can be scrutinized while the rest undergoes as normal interactions as possible. A high resolution scanning is possible in this way to help pinpoint the key residues responsible for an assembly or disassembly process under investigation.[51,52]

Our group in recent years developed a method to perform molecular imprinting in cross-linked surfactant micelles and the resulting MINPs are water-soluble nanoparticles ~5 nm in size,[53] among the smallest imprinted materials.[54,55] They can target both the hydrophobic residues[56] and acidic/basic ones,[57,58] and bind complex biological peptides with tens of nanomolar binding affinities.[59,60] As shown in Scheme 1, a peptide template in this method is first solubilized in water by the micelles of cross-linkable surfactant **1**, together with a small amount of 2,2-dimethoxy-2-phenylaceto-phenone (DMPA, a photo initiator). The surface of the micelle is cross-linked by diazide **2** via the highly efficient azide–alkyne click reaction, followed by another round of click reaction typically with monoazide **3a** for surface-functionalization. For peptide imprinting, a water-soluble free-radical cross-linker (*N*,*N*'-methylene-bisacrylamide or MBAm) is also included in the formulation. The hydrophobic radical initiator (DMPA) prefers to reside in the micellar core due to its hydropohbiciity. Once the initiating radical reacts with the methacrylate of

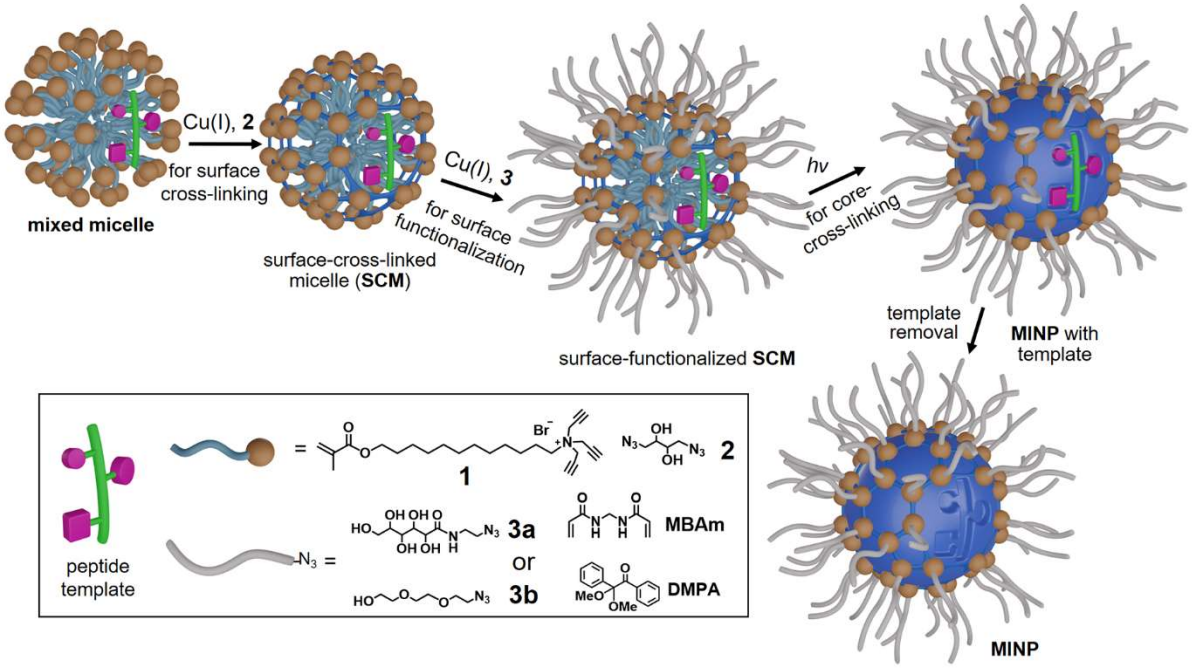

Scheme 1. Preparation of peptide-binding MINP by surface–core double cross-linking of the peptide-containing micelle of **1**.

the cross-linkable surfactant (**1**) in the surface-cross-linked micelle (SCM), the propagating radical is covalently confined within the micelle and can polymerize only those MBAm molecules diffused to the micelle. A belt of hydrogen-bonding amide groups will then form at the interface, with some covalently fixed around the peptide template residing in the same area by its amphiphilicity. MBAm is found to work as effectively as specially designed FMs for the molecular imprinting and binding of peptides[60] and increases the binding constant of 4-nitrophenyl-α-D-glucopyranoside by 180-fold.[61]

For our scanning, we divided $A\beta_{1\text{-}40}$ (H_2N-DAEFRHDSGY-EVHHQKLVFF-AEDVGSNKGA-IIGLMVGGVV-OH) into four equal segments, 10 residues in each. We then prepared four MINPs using each segment of peptide as the template. It is known that in $A\beta_{1\text{-}40}$ residues 10–22 and 30–40 form β strands and residues 23–29 adopt a loop structure to enable the two β strands to interact intramolecularly.[62] Thus, the four MINPs mainly target the flexible N-terminal tail, the internal β strand closer to the N-terminal, the loop region, and the β strand near the C-terminal, respectively. Since the MINPs could be added to an Aβ solution at different stages of the aggregation (Figure 1), we should be able to understand how binding of a specific sequence inhibits aggregation or reverses it at a particular stage.

Thioflavin T (ThT) represents the "gold standard" probe for monitoring Aβ fibrillation.[63] As it binds the fibrils, its emission maximum shifts from 445 nm to ~485 nm and its emission intensity increases by several orders of magnitude. MINPs are typically prepared with polyhydroxylated monoazide **3a** as the surface ligand for facile purification of the material by precipitation into acetone, followed by solvent washing. The resulting MINPs, however, strongly enhance the emission of ThT and thus interfere with its sensing of $A\beta_{1\text{-}40}$ fibrillization. Replacing the surface ligands with a tri(ethylene glycol)-derived azide **3b**, fortunately, eliminates the problem (Figure S4). The resulting MINPs were purified by dialysis (see Experimental Section for details).

Table 1 shows the binding properties of these MINPs characterized by isothermal titration calorimetry (ITC), one of the most reliable methods to study intermolecular interactions. MINPs typically contain approximately 50 cross-linked surfactants as estimated by dynamic light scattering (DLS). A surfactant/template ratio of 50:1, hence, should afford an average of one binding site per nanoparticle.[53] Consistent with the notion, ITC shows that most MINPs contain 1.0–1.3 binding site (*N*) per nanoparticle.

Table 1. Binding of Amyloid segments by MINPs determined by Isothermal titration calorimetry (ITC).[a]

Entry	MINP	peptide	K_a ($\times 10^5$ M^{-1})	-Δ*G* (kcal/mol)	*N* [b]	K_{rel} [b]
1	MINP($A\beta_{1-10}$)	$A\beta_{1-10}$	115.3 ± 32.7	8.67	1.30 ± 0.07	1
2	MINP($A\beta_{1-10}$)	$A\beta_{11-20}$	4.65 ± 0.22	6.96	1.12 ± 0.02	0.040
3	MINP($A\beta_{1-10}$)	$A\beta_{21-30}$	1.76 ± 0.12	6.44	1.29 ± 0.09	0.015
4	MINP($A\beta_{1-10}$)	$A\beta_{31-40}$	2.44 ± 0.23	6.61	1.05 ± 0.03	0.021
5	MINP($A\beta_{11-20}$)	$A\beta_{1-10}$	10.7 ± 1.47	8.38	0.84 ± 0.01	0.034
6	MINP($A\beta_{11-20}$)	$A\beta_{11-20}$	313.1 ± 21.7	9.20	1.20 ± 0.06	1
7	MINP($A\beta_{11-20}$)	$A\beta_{21-30}$	3.92 ± 0.29	7.61	1.04 ± 0.02	0.012
8	MINP($A\beta_{11-20}$)	$A\beta_{31-40}$	4.00 ± 0.21	7.62	0.97 ± 0.01	0.013
9	MINP($A\beta_{21-30}$)	$A\beta_{1-10}$	11.5 ± 0.67	8.33	0.62 ± 0.01	0.027
10	MINP($A\beta_{21-30}$)	$A\beta_{11-20}$	2.92 ± 1.89	7.45	0.81± 0.06	0.006
11	MINP($A\beta_{21-30}$)	$A\beta_{21-30}$	425.7 ± 26.2	9.36	1.12 ± 0.01	1
12	MINP($A\beta_{21-30}$)	$A\beta_{31-40}$	2.31 ± 0.83	7.32	1.10 ± 0.01	0.005
13	MINP($A\beta_{31-40}$)	$A\beta_{1-10}$	1.72 ± 1.31	7.74	0.74 ± 0.05	0.007
14	MINP($A\beta_{31-40}$)	$A\beta_{11-20}$	11.7 ± 3.42	8.38	1.20 ± 0.06	0.048
15	MINP($A\beta_{31-40}$)	$A\beta_{21-30}$	4.76 ± 1.26	7.15	0.80 ± 0.03	0.019
16	MINP($A\beta_{31-40}$)	$A\beta_{31-40}$	241.3 ± 26.8	9.06	1.22 ± 0.02	1
17	MINP($A\beta_{1-10}$)	$A\beta_{1-40}$	17.9 ± 1.3	7.67	1.07 ± 0.04	0.155
18	MINP($A\beta_{11-20}$)	$A\beta_{1-40}$	26.2 ± 2.4	7.88	0.98 ± 0.03	0.084
19	MINP($A\beta_{21-30}$)	$A\beta_{1-40}$	36.9 ± 4.3	8.06	0.99 ± 0.02	0.087
20	MINP($A\beta_{31-40}$)	$A\beta_{1-40}$	45.2 ± 1.9	8.17	1.31 ± 0.04	0.187
21	NINP [c]	$A\beta_{1-40}$	-	-	-	-

[a] The titrations were performed in HEPES buffer pH 7.4 at 298 K. [b] N is the average number of binding site per nanoparticle measured by ITC curve fitting. [b] K_{rel} is the relative binding constant of a guest normalized to that of the templating peptide for a particular MINP. [c] Nonimprinted nanoparticles (NINPs) are prepared following similar procedures for the MINPs, except without any templates.

Table 1 shows all four MINPs bind their corresponding templating peptides strongly. MINP($A\beta_{1-10}$), i.e., the MINP prepared with $A\beta_{1-10}$ as the template, for example, binds its template with a binding constant of $K_a = 115.3 \times 10^5\ M^{-1}$ in HEPES buffer (entry 1). The binding constant corresponds to nearly 9 kcal/mol of binding free energy. Similar but somewhat stronger bindings are observed for the other segments, by their own MINPs (entries 6, 11, and 16). Previous studies have shown that MINP binding of peptide is driven primarily by hydrophobic interactions and supplemented by hydrogen bonds.[56,60] In the current study, however, $A\beta_{21-30}$ shows the strongest binding (toward its own MINP receptor), followed by $A\beta_{11-20}$, $A\beta_{31-40}$, and lastly $A\beta_{1-10}$. Thus, the most hydrophobic $A\beta_{11-20}$ and $A\beta_{31-40}$ are bound with only mediocre affinities. A likely reason for this unusual trend is the self-association of these hydrophobic peptides. Truncated versions of Aβ have been shown to aggregate easily in aqueous solution, as long as at least one hydrophobic core is present in the structure.[64] Since the hydrophobic cores center around AA17–21 (LVFFA) and AA31–36 (IIGLMV), $A\beta_{11-20}$ and $A\beta_{31-40}$ are expected to aggregate to some extent before they were added into the MINP solution during our ITC titrations. MINP binding, under such a scenario, would need to compete with the self-aggregation of the peptide, making the apparent K_a lower than the true values for the binding of monomeric peptide. Consistent with the postulation, MINP binding for the full-length $A\beta_{1-40}$ is always weaker than for the peptide templates themselves (entries 17–20). The full-length peptide has a higher propensity of aggregation than the shorter segments. The corresponding measured binding constants, thus, are expected to decrease further due to stronger competition from the peptide self-aggregation. A control experiment shows that nonimprinted nanoparticles (NINPs) prepared without templates fail to bind $A\beta_{1-40}$ (entry 21), indicating that the binding affinity and selectivity were derived from molecular imprinting.

Table 1 also contains a column of K_{rel}, which is the relative binding constant of a guest normalized to that of the templating peptide for a particular MINP. K_{rel} thus by definition is 1 for the templating peptide and measures the selectivity of the MINP for its own template. Consistent with strong binding selectivities of MINPs for peptides,[59,60] very small K_{rel} values are observed for non-templating peptides, ranging from 0.015 to 0.040 with MINP($A\beta_{1-10}$) (entries 2–4). Similar observations are made with other MINPs (entries 5–16).

Inhibition of $A\beta_{1-40}$ aggregation. Encouraged by 20–90 nM apparent binding affinity of the MINPs for their targeted sequences and high selectivity, we studied their inhibition of $A\beta_{1-40}$ using ThT as the probe. Monomeric $A\beta_{1-40}$ was obtained from treating a lyophilized sample with hexafluoro-2-propanol (HFIP), followed by evaporation of the organic solvent and reconstitution of the residue with aqueous buffer.[16] As shown by Figure 2a (black curve), the sigmoidal curve for the ThT emission mirrors the aggregation curve illustrated in Figure 1, with a lag time of approximately 100 min under our experimental conditions. Addition of 0.1 equiv. of the MINP receptors noticeably delays the onset of the polymerization phase, as well as the end fluorescence intensity, indicating that all the nanoparticles slow down the aggregation of the amyloid peptide and reduce the amounts of fibrils formed. The kinetic effects and the thermodynamic effects mostly go hand in hand although cross-overs are also observed. Among the four receptors, MINP($A\beta_{21-30}$) is clearly the most able to slow down the aggregation (as judged by the delayed onset of the polymerization phase) and inhibit fibril formation (as judged by the reduced end fluorescence intensity), followed by MINP($A\beta_{31-40}$). MINP($A\beta_{1-10}$) and MINP($A\beta_{11-20}$) display a crossover in the inhibition: whereas MINP($A\beta_{1-10}$) better slows down the aggregation, MINP($A\beta_{11-20}$) gives a slightly lower end fluorescence for ThT. We used $A\beta_{1-40}$ primarily in this study. When a similar experiment was performed with the more aggregation-prone $A\beta_{1-42}$, a shorter lag time was observed but the basic trend of the MINPs stayed the same (Figure S10).

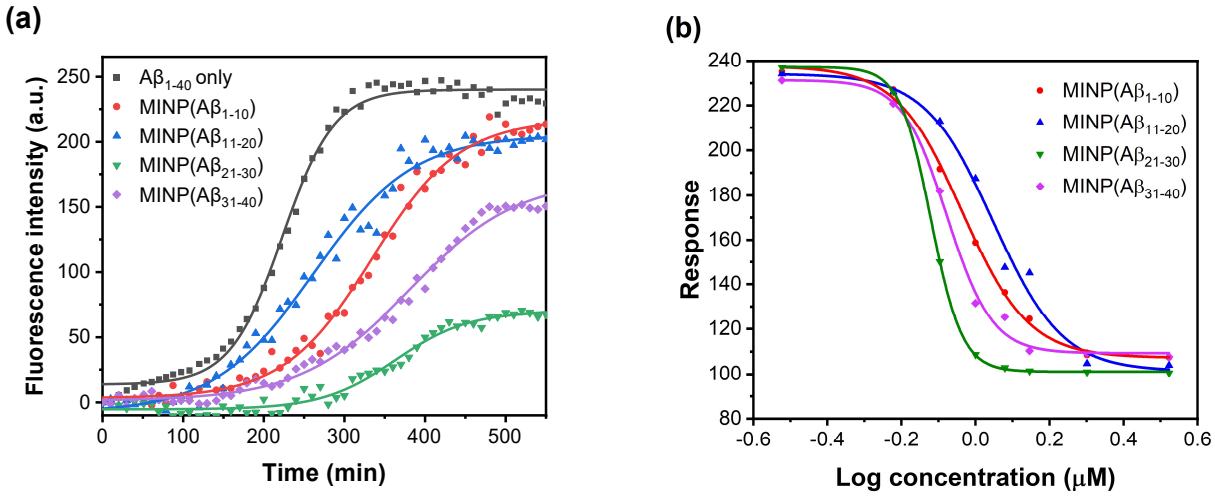

Figure 2. (a) ThT emission intensity at 485 nm in the presence of $A\beta_{1-40}$ and different MINP inhibitors. [$A\beta_{1-40}$] = 10 μM. [MINP] = 1.0 μM. [ThT] = 100 μM. The peptide was incubated at 37 ˚C in HEPES buffer (pH 7.4). The smooth curves were obtained by nonlinear least squares curve fitting of the emission intensity to the Hill equation. (b) Dose-response curves for the inhibition of $A\beta_{1-40}$ aggregation using different MINPs. The experiments were performed in duplicates and the errors between the runs were <10%.

We then performed similar inhibition experiments using different concentrations of the MINPs and obtained the dose-response curves (Figure 2a). The half maximal inhibitory concentration (IC_{50}) for the four MINPs were found to be 0.92 ± 0.016 μM for MINP($A\beta_{1-10}$), 1.11±0.049 μM for MINP($A\beta_{11-20}$), 0.76 ± 0.01 μM for MINP($A\beta_{21-30}$), and 0.83 ± 0.02 μM for MINP($A\beta_{31-40}$). When the full curves are compared, MINP($A\beta_{21-30}$) clearly has the strongest inhibitory effect on the aggregation of the monomer, followed by MINP($A\beta_{31-40}$), MINP($A\beta_{1-10}$), and MINP($A\beta_{11-20}$), respectively (Figure 2b).

We also studied the effects of the MINPs on the $A\beta_{1-40}$ aggregation using AFM. Figure 3a shows that, after 400 minutes of incubation, $A\beta_{1-40}$ gives large amounts of fibrous structures many microns in length. All the MINPs substantially reduce the fibrils formed. Meanwhile, smaller, spherical structures appear in the AFM images (Figures 3b–d). Most notably, at a 1:10 molar ratio to the Aβ peptide, MINP($A\beta_{21-30}$) nearly completely suppresses the fibril formation, affording only small amounts of

spherical aggregates (Figure 3d). Formation of β-sheets can be monitored by CD spectroscopy.[65] Consistent with the AFM study, all MINPs were able to reduce the negative band at 218 nm of incubated $A\beta_{1-40}$ samples that correspond to the β sheets, and MINP($A\beta_{21-30}$) was clearly the best (Figure S11).

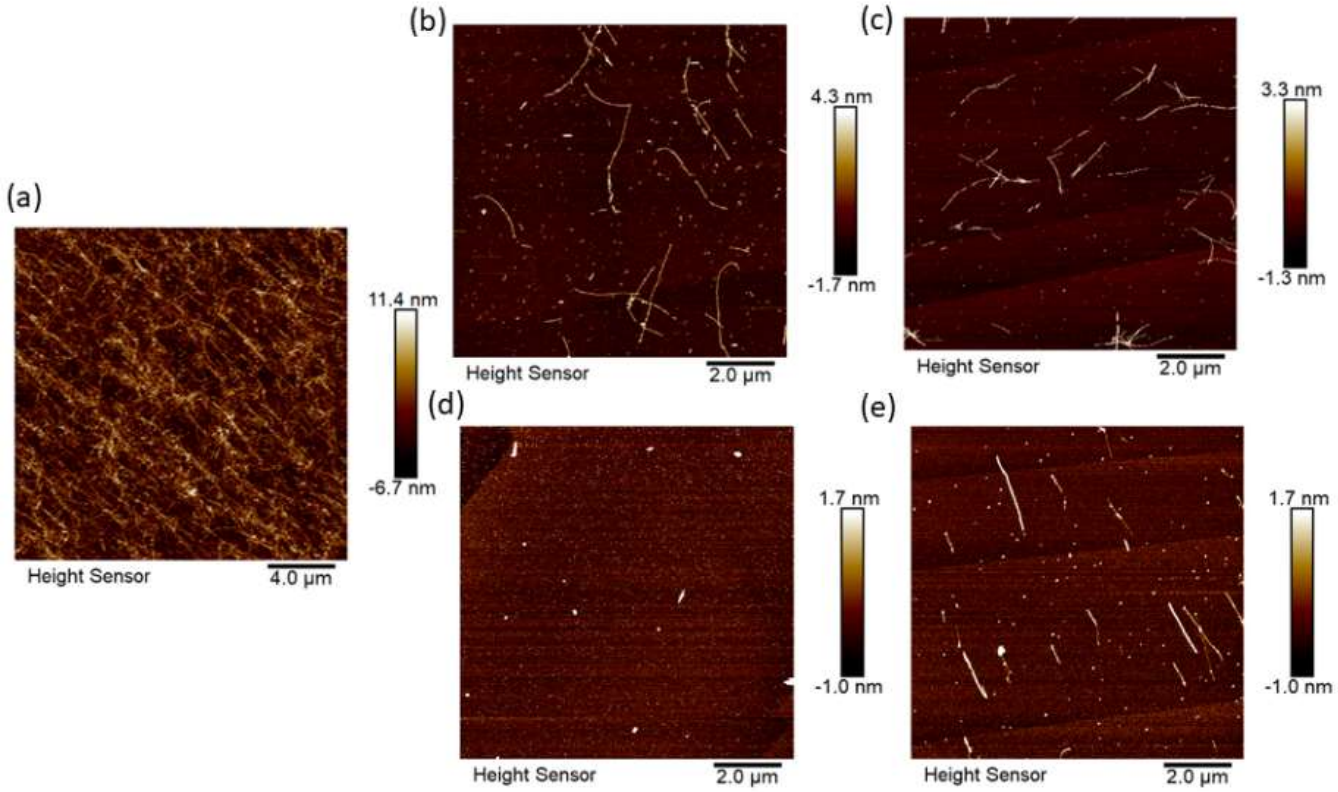

Figure 3. AFM study of $A\beta_{1-40}$ aggregation using (a) no inhibitor, (b) MINP($A\beta_{1-10}$), (c) MINP($A\beta_{11-20}$), (d) MINP($A\beta_{21-30}$), (e) MINP($A\beta_{31-40}$). [$A\beta_{1-40}$] = 10 µM. [MINP] = 1.0 µM. AFM images were recorded after 400 minutes of incubation of $A\beta_{1-40}$ at 37 ˚C in HEPES buffer (pH 7.4).

Therefore, all three techniques (i.e., fluorescence spectroscopy, AFM imaging, and CD spectroscopy) suggest the most effective way to inhibit $A\beta_{1-40}$ aggregation—as least along the pathway to fibril formation—is to bind $A\beta_{21-30}$, followed by $A\beta_{31-40}$. The effect of binding $A\beta_{31-40}$ is reasonable given the known, strong contribution of residues 31–36 (IIGLMV) to the Aβ aggregation.[7] The strongest inhibitory effect of binding $A\beta_{21-30}$, however, might appear counterintuitive, as the second strongest contributor to the Aβ aggregation is AAs 17–21 (LVFFA).[7]

Since residues 10–22 and 30–40 are β strands and residues 23–29 form a loop for the U-turned $A\beta_{1\text{-}40}$,[62] our scanning indicates that binding the loop is the most effective way to inhibit Aβ aggregation. There could be at least two reasons for this result. First, the loop region is key to the formation of the turn structure of amyloid peptide, with an intramolecular salt bridge between D23 and K28 stabilizing the turn.[6,9] MINP binding at this region is expected to unfold the U-turned β-sheet, making it unable to follow the normal pathway for aggregation. Second, although binding the β strands (at residues 10–22 and 30–40) can also inhibit the aggregation, the MINP binding would have to compete with both intra- and intermolecular β-sheet formation. As shown in our ITC studies, (intermolecular) self-aggregation of the amyloid peptides compete with the MINP binding and reduces the apparent binding constant if the MINP targets the most hydrophobic segments of the peptide.

Both MINP($A\beta_{11\text{-}20}$) and MINP($A\beta_{31\text{-}40}$) target the hydrophobic β strands of the peptide. Our data shows that binding the more extensive C-terminal β strand has a stronger inhibitory effect on the aggregation than binding the shorter internal strand. The C-terminal strand has a high aggregation propensity, evident from its β-sheet formation independent of pH, solvent, or temperature.[66] Its binding by MINP thus eliminates one of the strongest drivers for the Aβ aggregation. The stronger binding for the parent peptide by MINP($A\beta_{31\text{-}40}$) over MINP($A\beta_{11\text{-}20}$) can also be helpful in this competition (Table 1, entries 9 and 11).

Disassembly of $A\beta_{1\text{-}40}$ Aggregates Amyloid disaggregation happens naturally, often through chaperone protein disaggregase and is considered a potential treatment to amyloid peptide-related diseases.[67] The process requires chemical energy from ATP to disassemble amyloid fibrils, followed by proteolysis. In our case, the disassembly is driven by a strong binding of the MINP for the peptide, which competes with the inter- and intramolecular interactions of Aβ.

We studied the reversal of Aβ aggregation at two different stages. In the first set of experiments, 10 μM $A\beta_{1\text{-}40}$ was incubated with ThT at 37 ˚C in HEPES buffer (pH 7.4) for 240 min. As shown by Figure 4 (the black, control curve), the peptides is in the middle of the polymerization phase at this time,

already aggregated. Addition of 4 μM of different MINPs can all reverse the aggregation but their effects differ greatly. Among the four receptors, MINP($A\beta_{11-20}$) is the clear winner, not only lowering the ThT emission most rapidly but also keeping the end fluorescence to the lowest level, similar to that of the initial value of the control. MINP($A\beta_{21-30}$) displays a lag phase in the inhibition, showing almost no effects for about 100 minutes before a quick reduction occurs but the end fluorescence of ThT remains quite high. The other two nanoparticles, MINP($A\beta_{1-10}$) and MINP($A\beta_{31-40}$) are both slow to act, although MINP($A\beta_{1-10}$) lowers the ThT emission more than MINP($A\beta_{31-40}$) at the end of the experiments.

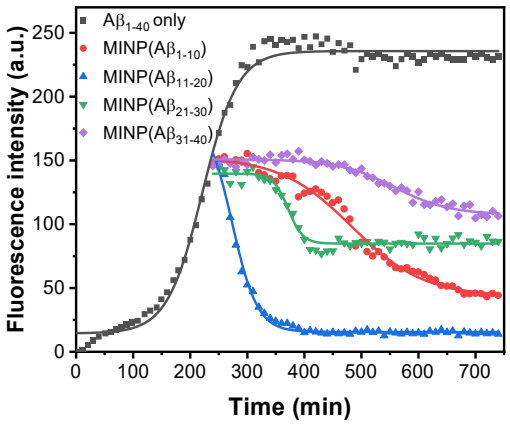

Figure 4. ThT emission intensity at 485 nm in the presence of $A\beta_{1-40}$ and different MINP inhibitors, with 4.0 μM of MINP added after the peptide was incubated for 240 min at 37 ˚C in HEPES buffer (pH 7.4). [$A\beta_{1-40}$] = 10 μM. [ThT] = 100 μM. The experiments were performed in duplicates and the errors between the runs were <10%. The smooth curves were obtained by nonlinear least squares curve fitting of the emission intensity to the Hill equation.

AFM showed a similar trend. Different MINP receptors were added to the $A\beta_{1-40}$ peptide that had been preincubated for 240 min. After another 700 min, AFM imaging shows that the sample containing MINP($A\beta_{11-20}$) gives the least amounts of fibril materials (Figure 5c). Although all samples show less fibril formation that the control (Figure 5a), the inhibitory effects more or less follow those observed in the fluorescence study—i.e., MINP($A\beta_{11-20}$) > MINP($A\beta_{1-10}$) > MINP($A\beta_{21-30}$) ≈

MINP($A\beta_{31-40}$). A similar trend was observed in the CD spectroscopy (Figure S12), except MINP($A\beta_{31-40}$) being more effective than MINP($A\beta_{21-30}$).

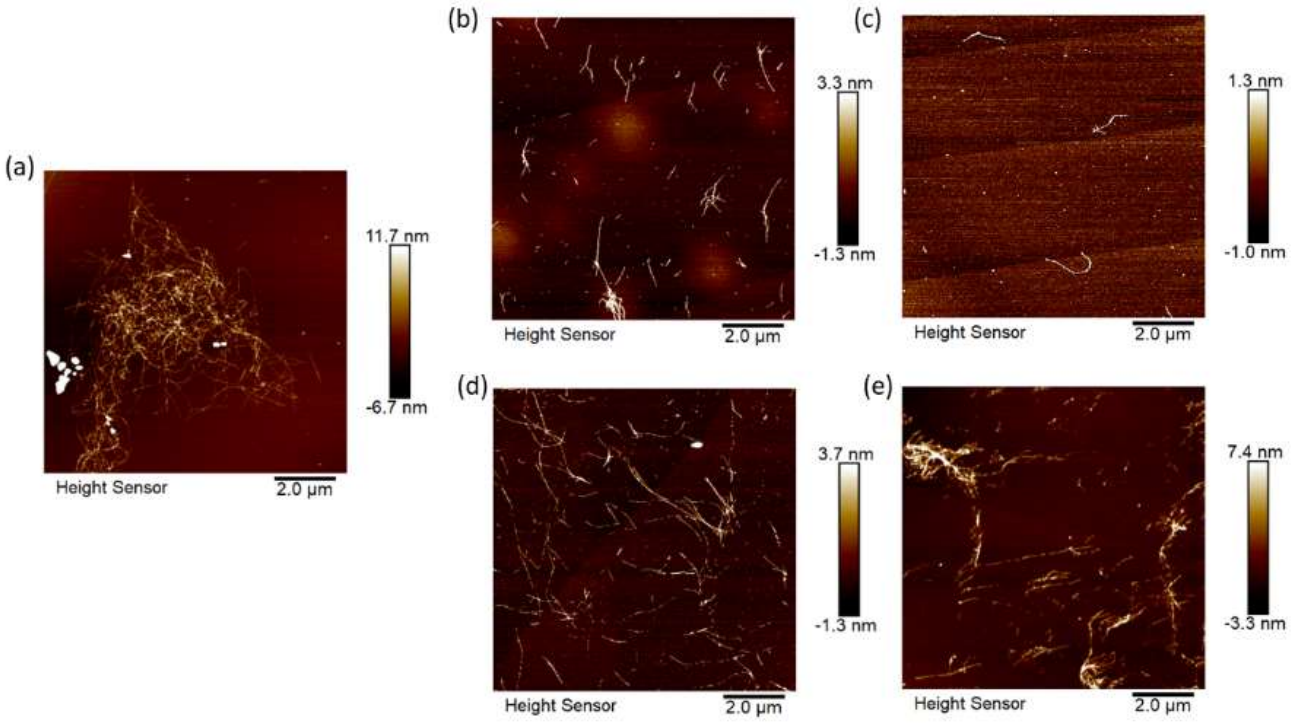

Figure 5. AFM images of $A\beta_{1-40}$ peptide recorded after 700 min of incubation with (a) no inhibitor, (b) MINP($A\beta_{1-10}$), (c) MINP($A\beta_{11-20}$), (d) MINP($A\beta_{21-30}$), (e) MINP($A\beta_{31-40}$). [$A\beta_{1-40}$] = 10 µM. [MINP] = 4.0 µM. The peptides were pre-incubated at 37 ˚C in HEPES buffer (pH 7.4) for 240 min before the MINP addition.

It is intriguing that binding the β strand closer to the N terminal is the most powerful way to reverse Aβ aggregation during the polymerization phase. In comparison to other receptors, MINP($A\beta_{11-20}$) is not only faster acting (Figure 4) but also more completely wipes out the fibrous structures (Figure 5). During the polymerization phase, the intermediate aggregates are in dynamic exchange with the oligomers while growing into longer, more mature fibrils.[11] Since the C-terminal β strand has the highest aggregation propensity in the whole peptide,[66] it should already be engaged in extensive intra- and intermolecular interactions in the polymerization phase. Consistent with this picture, binding $A\beta_{31-40}$ is the least effective way to reverse the polymerization, whether from the kinetic or thermodynamic point of view (Figure 4,

purple curve). The fast action of MINP($A\beta_{11-20}$) suggests that this strand is still readily accessible to the MINP receptor, whether directly from the intermediate fibrils or the oligomers that exchange with these fibrils. Although the flexible N-terminal tail (AA 1–10) is also accessible, the β strand near AA 11–20 is a much stronger contributor to the fibril formation and thus its binding should be more detrimental to the fibril growth.

We then performed similar experiments, but with the $A\beta_{1-40}$ peptide pre-incubated for 400 min before the MINP receptors were added so that the fibrils were already in the saturation phase. One noticeable observation in these disassembly experiments is that, as the amyloid peptide is allowed to aggregate further, it takes a larger amounts of MINP receptors to reverse the process. For example, when the MINP is added in the beginning of the aggregation process, 0.1 equiv. of the MINP could strongly inhibit the aggregation (Figure 2a). If the MINP is added in the middle of the polymerization phase (at 240 min), 0.4 equiv. of the receptor are needed (Figure 4). When the MINP is added at the saturation phase (at 400 min), even 0.4 equivalents of MINP are insufficient (Figure 6a) and 0.8 equivalents of MINP are necessary (Figure 6b). According to Figure 6b, the inhibitory effects of the MINP are the strongest for MINP($A\beta_{1-10}$), followed by MINP($A\beta_{11-20}$), MINP($A\beta_{31-40}$), and MINP($A\beta_{21-30}$), respectively. The results are also supported by the AFM imaging, which shows more or less a similar trend even through all MINPs could reduce the amounts of fibrils formed (Figure 7). Figure 6b shows that MINP($A\beta_{1-10}$) and MINP($A\beta_{11-20}$) are faster acting than MINP($A\beta_{31-40}$) and MINP($A\beta_{21-30}$). Consistent with the fluorescence assays, when AFM images are taken at intermediate times (Figure S13c/d for 600 min and Figure S14c/d for 800 min of incubation time), significantly more fibrils are observed than those at the end (Figure 7d/e) for the samples treated with MINP($A\beta_{31-40}$) and MINP($A\beta_{21-30}$). Thus, disaggregation is quite slow. In contrast, as shown by Figures S13a/b, S14a/b, and Figure b/c, the intermediate and the final images are very similar in case of MINP($A\beta_{1-10}$) and MINP($A\beta_{11-20}$), suggesting disaggregation happens at a faster rate.

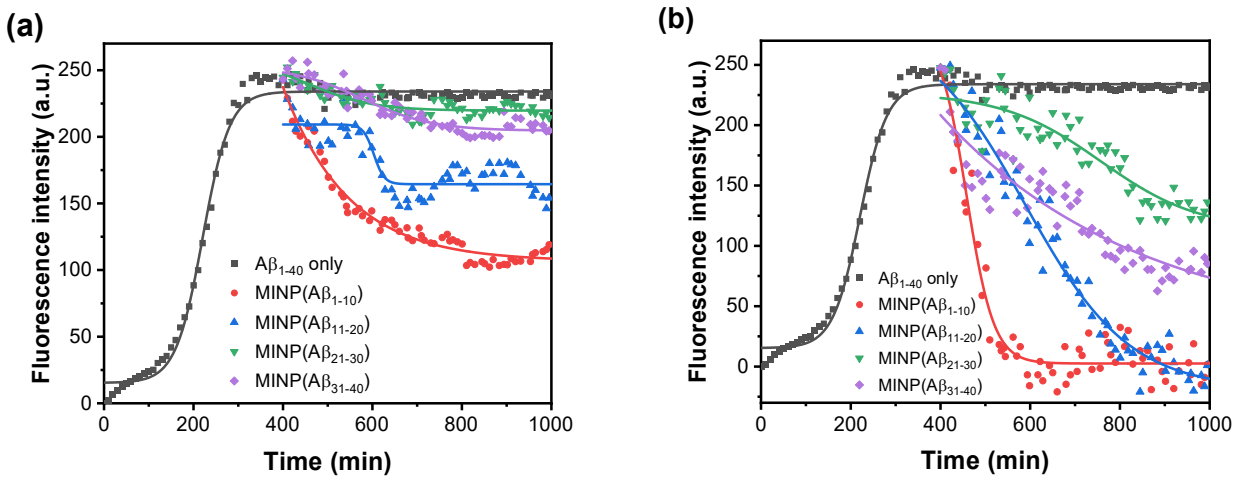

Figure 6. ThT emission intensity at 485 nm in the presence of $A\beta_{1\text{-}40}$ and different MINP inhibitors, with (a) 1.0 μM of MINP and (b) and 8.0 μM of MINP added after the peptide was incubated for 400 min at 37 ˚C in HEPES buffer (pH 7.4). $[A\beta_{1\text{-}40}]$ = 10 μM. [ThT] = 100 μM. The experiments were performed in duplicates and the errors between the runs were <10%. The smooth curves were obtained by nonlinear least squares curve fitting of the emission intensity to the Hill equation.

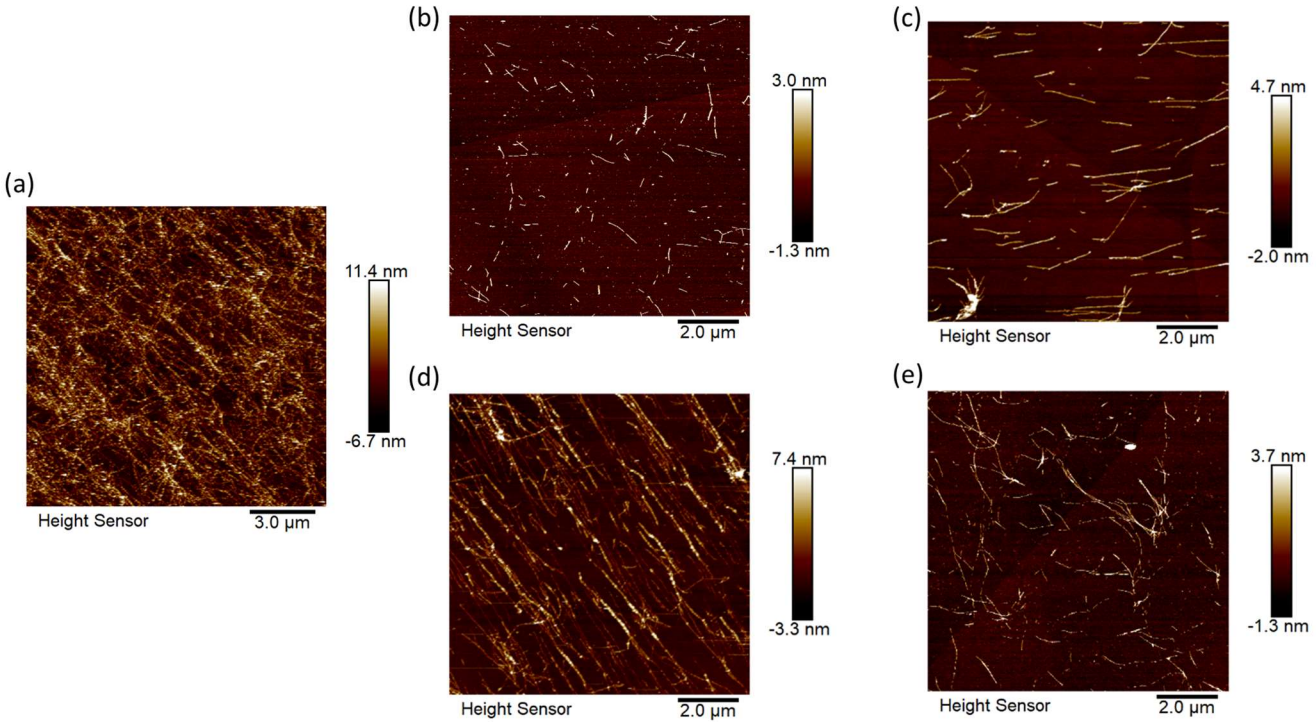

Figure 7. AFM images of $A\beta_{1\text{-}40}$ peptide recorded after 1000 min of incubation with (a) no inhibitor, (b) MINP($A\beta_{1\text{-}10}$), (c) MINP($A\beta_{11\text{-}20}$), (d) MINP($A\beta_{21\text{-}30}$), (e) MINP($A\beta_{31\text{-}40}$). $[A\beta_{1\text{-}40}]$ = 10 μM. [MINP] =

8.0 μM. The peptides were pre-incubated at 37 ˚C in HEPES buffer (pH 7.4) for 400 min before the MINP addition.

It is interesting that, whereas the best target to reverse the aggregation is the internal β strand in the polymerization phase, binding the flexible N-terminal tail is the most effective in the saturation phase. This tail has been shown by solid-state NMR spectroscopy to be structurally disordered in $A\beta_{1\text{-}40}$ fibrils,[6] and thus contribute the least to the stability of the fibrils. However, the more mature the aggregates, the more fully locked are the other key residues involved in the folded β strands, including the loop. The MINP binding not only has to overcome a tremendous thermodynamic barrier to bind these segments, their accessibility should also be the lowest. Meanwhile, the exposed, more flexible N-terminal tail becomes the only ligand available to the MINP. If sufficient amounts of MINP are present, they essentially grab $A\beta_{1\text{-}40}$ by this tail and probably by their shear size disassemble the aggregates. Molecular chaperones such as Hsp 70s perform a range of functions including unfold and solubilize protein aggregates. An mechanism of "entropic pulling" has been proposed for its action, in which Hsp 70 finds more freedom as it pulls the peptide tail away from the aggregates.[68] It is possible MINP acts in a similar fashion.

Conclusions

With their nanodimension and strong/selective binding for peptides, MINPs enable us to scan the four different segments of $A\beta_{1\text{-}40}$, the flexible N-terminal tail (AA1–10), the internal β strand closer to the N-terminal (AA11–20), the loop region (AA21–30), and the β strand near the C-terminal (AA31–40), respectively. The earlier the peptide binder is added to intervene amyloid peptide aggregation, the less amount of material is required. When the MINP is added at the monomer stage, all the amino acids are largely accessible to the MINP and the most effective sequence to target is the loop. Its binding unfolds the peptide and prohibits the intermolecular U-turned structure of the amyloid fiber, which is key to the aggregation. The second best choice is the highly hydrophobic C-terminal β strand, likely because its binding removes one of the largest drivers for the aggregation.

In the polymerization phase, the best target is the β strand near the N-terminal and, in the saturation phase, the N-terminal flexible tail. The change of target likely derives from a tradeoff between the accessibility of the amino acids to the MINP receptor and the importance of these residues to the overall aggregation. In the polymerization phase, both the N-terminal tail and its nearby β strand are accessible to the MINP, but the latter is a far more important contributor to the fibril formation. As the $A\beta_{1\text{-}40}$ moves to the saturation phase, tighter β sheets are formed which greatly increase the energetic costs of MINP binding with those residues already involved in the β sheet formation. A higher amount of MINP is needed to dissemble the aggregates and accessibility becomes the dominant factor. In this last situation, the best target is the exposed, structureless N-terminal tail, followed by the less tightly bound β strand near the N-terminal.

It is encouraging that peptide-binding "nanoscanners" can be used to probe the functional roles of a long peptide. From a biological point of view, the loop region of the beta amyloid peptides is the most promising target to prevent aggregation. Once the aggregation starts, the therapeutic reagent will need to account for a shift of target at different time frame. Since amyloid peptides/proteins are involved in numerous diseases,[1,2] we hope that similar scanning can help identify potential drug targets on other peptides/proteins as well.

Experimental Section

General Experimental Methods. All organic solvents and reagents were of ACS-certified grade or higher grade and were purchased from commercial suppliers. Peptides were purchased from Biomatik with purity > 95% in the lyophilized form. Biotech-grade dialysis tubing (MW-cutoff (MWCO) of 5000 Da) was purchased from Spectrum Chemical. Chemicals shifts are reported in ppm relative to residual solvent peaks. NMR spectra were recorded on a Varian VXR-400 spectrometer. Chemicals shifts are reported in ppm relative to residual solvent peaks ($CDCl_3$ = 7.26 ppm for ^1H NMR). Coupling constants are reported in hertz. Milli-Q water (18.2 MU; Millipore Co., USA) was used for MINP preparation and all buffers. Dynamic light scattering (DLS) data were collected on a Malvern Zetasizer Nano ZS at 25 °C.

ITC was performed using a MicroCal VP-ITC Microcalorimeter with Origin 7 software and VPViewer2000 (GE Healthcare, Northampton, MA). Fluorescence spectra were recorded on a Varian Cary Eclipse Fluorescence spectrophotometer. CD spectra were measured on a Jasco J-715 CD Spectrometer.

Syntheses of surfactant **1**,[53] cross-linker **2**,[69] and surface ligand **3a**,[53] and **3b**,[70] were reported previously.

Preparation of MINP. To a micellar solution of surfactant **1** (9.3 mg, 0.02 mmol) in H_2O (2.0 mL), *N*,*N*'-methylene-bisacrylamide (MBAm, 10 μL of a 2 mmol/mL solution in DMSO, 0.02 mmol), desired peptide in H_2O (10 μL of a solution of 0.04 mmol/mL, 0.0004 mmol), and 2,2-dimethoxy-2-phenylacetophenone (DMPA,10 μL of a 12.8 mg/mL solution in DMSO, 0.0005 mmol) were added. The mixture was subjected to ultrasonication for 10 min before compound **2** (4.13 mg, 0.024 mmol), $CuCl_2$ (10 μL of a 6.7 mg/mL solution in H_2O, 0.0005 mmol), and sodium ascorbate (10 μL of a 99 mg/mL solution in H_2O, 0.005 mmol) were added. After the reaction mixture was stirred slowly at room temperature for 12 h, compound **3b** (7 mg, 0.04 mmol), $CuCl_2$ (10 μL of a 6.7 mg/mL solution in H_2O, 0.0005 mmol l), and sodium ascorbate (10 μL of a 99 mg/mL solution in H_2O, 0.005 mmol) were added. After being stirred for another 6 h at room temperature, the reaction mixture was transferred to a glass vial, purged with nitrogen for 15 min, sealed with a rubber stopper, and irradiated in a Rayonet reactor for 12 h. The reaction mixture was transferred into a dialysis tubing with a MW-cutoff (MWCO) of 5000 Da. The tubing dialyzed against 20 mL of methanol for 3 h and then 20 mL of water for 3 h, with the external solvent replaced every 30 min. The solution inside was lyophilized to give an off-white power (typical yields > 80%).

ThT fluorescence assay. The ThT assay was performed according to a standard procedure.[16] For the generation of amyloid monomers, the lyophilized $A\beta_{1\text{-}40}$ peptides were treated with hexafluoro-2-propanol (HFIP) to a concentration of 1 mg/mL. The solution was sonicated for 15 min, filtered through a 0.22 μm membrane filter to remove any preformed aggregates and dried under vacuum. Monomeric $A\beta_{1\text{-}40}$ was diluted in HEPES buffer (pH 7.4). Different concentrations of MINPs were mixed with 10 μM

$A\beta_{1-40}$ solution and incubated with 100 μM ThT in quartz cuvettes with 1.0 cm optical path at 37 ºC. ThT emission was monitored over time with the excitation wavelength of 450 nm and the emission wavelength of 485 nm.

Determination of binding constants by ITC. In general, a solution of an appropriate guest in 10 mM HEPES buffer (pH 7.4) was injected in equal steps into 1.43 mL of the corresponding MINP in the same solution. The top panel shows the raw calorimetric data. The area under each peak represents the amount of heat generated at each ejection and is plotted against the molar ratio of the MINP to the guest. The solid line is the best fit of the experimental data to the sequential binding of *N* equal and independent binding site on the MINP. The heat of dilution for the substrate, obtained by adding the substrate to the buffer, was subtracted from the heat released during the binding. Binding parameters were auto generated after curve fitting using Microcal Origin 7. All titrations were performed in duplicates and the errors between the runs were <10%.

ASSOCIATED CONTENT

Supporting Information

Characterization of MINPs, ITC titration curves, and CD spectra (PDF). This material is available free of charge via the Internet at http://pubs.acs.org.

AUTHOR INFORMATION

Corresponding Author

*E-mail: zhaoy@iastate.edu

Notes

The authors declare no competing financial interest.

Acknowledgments

We thank NSF (DMR-2002659) for financial support of this research.

References

(1) Eisenberg, D.; Jucker, M. The Amyloid State of Proteins in Human Diseases. *Cell* **2012**, *148*, 1188-1203.

(2) Hamley, I. W. The Amyloid Beta Peptide: A Chemist's Perspective. Role in Alzheimer's and Fibrillization. *Chem. Rev.* **2012**, *112*, 5147-5192.

(3) Hardy, J. A.; Higgins, G. A. Alzheimer's Disease: The Amyloid Cascade Hypothesis. *Science* **1992**, *256*, 184-185.

(4) Bernstein, S. L.; Dupuis, N. F.; Lazo, N. D.; Wyttenbach, T.; Condron, M. M.; Bitan, G.; Teplow, D. B.; Shea, J.-E.; Ruotolo, B. T.; Robinson, C. V.; Bowers, M. T. Amyloid-B Protein Oligomerization and the Importance of Tetramers and Dodecamers in the Aetiology of Alzheimer'S Disease. *Nat. Chem.* **2009**, *1*, 326.

(5) Bucciantini, M.; Giannoni, E.; Chiti, F.; Baroni, F.; Formigli, L.; Zurdo, J.; Taddei, N.; Ramponi, G.; Dobson, C. M.; Stefani, M. Inherent Toxicity of Aggregates Implies a Common Mechanism for Protein Misfolding Diseases. *Nature* **2002**, *416*, 507-511.

(6) Petkova, A. T.; Ishii, Y.; Balbach, J. J.; Antzutkin, O. N.; Leapman, R. D.; Delaglio, F.; Tycko, R. A Structural Model for Alzheimer's Beta -Amyloid Fibrils Based on Experimental Constraints from Solid State Nmr. *Proc. Natl. Acad. Sci. U. S. A.* **2002**, *99*, 16742-16747.

(7) Fernandez-Escamilla, A.-M.; Rousseau, F.; Schymkowitz, J.; Serrano, L. Prediction of Sequence-Dependent and Mutational Effects on the Aggregation of Peptides and Proteins. *Nat. Biotechnol.* **2004**, *22*, 1302-1306.

(8) Lührs, T.; Ritter, C.; Adrian, M.; Riek-Loher, D.; Bohrmann, B.; Döbeli, H.; Schubert, D.; Riek, R. 3d Structure of Alzheimer's Amyloid-B(1-42) Fibrils. *Proceedings of the National Academy of Sciences* **2005**, *102*, 17342-17347.

(9) Zheng, J.; Jang, H.; Ma, B.; Tsai, C.-J.; Nussinov, R. Modeling the Alzheimer Aβ17-42 Fibril Architecture: Tight Intermolecular Sheet-Sheet Association and Intramolecular Hydrated Cavities. *Biophys. J.* **2007**, *93*, 3046-3057.

(10) Yang, Y.; Arseni, D.; Zhang, W.; Huang, M.; Lövestam, S.; Schweighauser, M.; Kotecha, A.; Murzin, A. G.; Peak-Chew, S. Y.; Macdonald, J.; Lavenir, I.; Garringer, H. J.; Gelpi, E.; Newell, K. L.; Kovacs, G. G.; Vidal, R.; Ghetti, B.; Ryskeldi-Falcon, B.; Scheres, S. H. W.; Goedert, M. Cryo-Em Structures of Amyloid-B 42 Filaments from Human Brains. *Science* **2022**, *375*, 167-172.

(11) Michaels, T. C. T.; Šarić, A.; Curk, S.; Bernfur, K.; Arosio, P.; Meisl, G.; Dear, A. J.; Cohen, S. I. A.; Dobson, C. M.; Vendruscolo, M.; Linse, S.; Knowles, T. P. J. Dynamics of Oligomer Populations Formed During the Aggregation of Alzheimer's Aβ42 Peptide. *Nat. Chem.* **2020**, *12*, 445-451.

(12) Landau, M.; Sawaya, M. R.; Faull, K. F.; Laganowsky, A.; Jiang, L.; Sievers, S. A.; Liu, J.; Barrio, J. R.; Eisenberg, D. Towards a Pharmacophore for Amyloid. *PLoS Biol.* **2011**, *9*, e1001080.

(13) Bhasikuttan, A. C.; Mohanty, J. Detection, Inhibition and Disintegration of Amyloid Fibrils: The Role of Optical Probes and Macrocyclic Receptors. *Chem. Commun.* **2017**, *53*, 2789-2809.

(14) Zhou, Z.; Gu, Y.-Q.; Wang, H.-X. Artificial Chiral Interfaces against Amyloid-B Peptide Aggregation: Research Progress and Challenges. *ACS Chem. Neurosci.* **2021**, *12*, 4236-4248.

(15) Song, Y.; Moore, E. G.; Guo, Y.; Moore, J. S. Polymer–Peptide Conjugates Disassemble Amyloid B Fibrils in a Molecular-Weight Dependent Manner. *J. Am. Chem. Soc.* **2017**, *139*, 4298-4301.

(16) Zhao, J.; Li, K.; Wan, K.; Sun, T.; Zheng, N.; Zhu, F.; Ma, J.; Jiao, J.; Li, T.; Ni, J.; Shi, X.; Wang, H.; Peng, Q.; Ai, J.; Xu, W.; Liu, S. Organoplatinum-Substituted Polyoxometalate Inhibits B-Amyloid Aggregation for Alzheimer's Therapy. *Angew. Chem. Int. Ed.* **2019**, *58*, 18032-18039.

(17) Xu, Z.; Jia, S.; Wang, W.; Yuan, Z.; Jan Ravoo, B.; Guo, D.-S. Heteromultivalent Peptide Recognition by Co-Assembly of Cyclodextrin and Calixarene Amphiphiles Enables Inhibition of Amyloid Fibrillation. *Nat. Chem.* **2019**, *11*, 86-93.

(18) Liu, H.; Qian, C. Y.; Yang, T.; Wang, Y. Q.; Luo, J.; Zhang, C. L.; Wang, X. H.; Wang, X. Y.; Guo, Z. J. Small Molecule-Mediated Co-Assembly of Amyloid-Beta Oligomers Reduces Neurotoxicity through Promoting Non-Fibrillar Aggregation. *Chem. Sci.* **2020**, *11*, 7158-7169.

(19) Zheng, Y.; Wang, P.; Li, S.; Geng, X.; Zou, L.; Jin, M.; Zou, Q.; Wang, Q.; Yang, X.; Wang, K. Development of DNA Aptamer as a B-Amyloid Aggregation Inhibitor. *ACS Appl. Bio Mater.* **2020**, *3*, 8611-8618.

(20) Geng, H.; Pan, Y. C.; Zhang, R.; Gao, D.; Wang, Z. J.; Li, B. Y.; Li, N.; Guo, D. S.; Xing, C. F. Binding to Amyloid-Beta Protein by Photothermal Blood-Brain Barrier-Penetrating Nanoparticles for Inhibition and Disaggregation of Fibrillation. *Adv. Funct. Mater.* **2021**, *31*.

(21) Maity, D.; Howarth, M.; Vogel, M. C.; Magzoub, M.; Hamilton, A. D. Peptidomimetic-Based Vesicles Inhibit Amyloid-Beta Fibrillation and Attenuate Cytotoxicity. *J. Am. Chem. Soc.* **2021**, *143*, 3086-3093.

(22) Wang, H.; Xu, X. X.; Pan, Y. C.; Yan, Y. X.; Hu, X. Y.; Chen, R. W.; Ravoo, B. J.; Guo, D. S.; Zhang, T. Recognition and Removal of Amyloid-Beta by a Heteromultivalent Macrocyclic Coassembly: A Potential Strategy for the Treatment of Alzheimer's Disease. *Adv. Mater.* **2021**, *33*.

(23) Xin, Y.; Wang, S.; Liu, H.; Ke, H.; Tian, S.; Cao, Y.; Huang, Y.; Shang, Y.; Jia, H.; Su, L.; Yang, X.; Meng, F.; Luo, L. Hierarchical Vitalization of Oligotyrosine in Mitigating Islet Amyloid Polypeptide Amyloidogenesis through Multivalent Macromolecules with Conformation-Restrained Nanobody Ligands. *ACS Nano* **2021**, *15*, 13319-13328.

(24) Wang, W.; Zhao, G.; Dong, X.; Sun, Y. Unexpected Function of a Heptapeptide-Conjugated Zwitterionic Polymer That Coassembles into B-Amyloid Fibrils and Eliminates the Amyloid Cytotoxicity. *ACS Appl. Mater. Interfaces* **2021**, *13*, 18089-18099.

(25) Aliyan, A.; Cook, N. P.; Martí, A. A. Interrogating Amyloid Aggregates Using Fluorescent Probes. *Chem. Rev.* **2019**, *119*, 11819-11856.

(26) Salveson, P. J.; Haerianardakani, S.; Thuy-Boun, A.; Yoo, S.; Kreutzer, A. G.; Demeler, B.; Nowick, J. S. Repurposing Triphenylmethane Dyes to Bind to Trimers Derived from Aβ. *J. Am. Chem. Soc.* **2018**, *140*, 11745-11754.

(27) Jiang, B.; Aliyan, A.; Cook, N. P.; Augustine, A.; Bhak, G.; Maldonado, R.; Smith McWilliams, A. D.; Flores, E. M.; Mendez, N.; Shahnawaz, M.; Godoy, F. J.; Montenegro, J.; Moreno-Gonzalez, I.;

Martí, A. A. Monitoring the Formation of Amyloid Oligomers Using Photoluminescence Anisotropy. *J. Am. Chem. Soc.* **2019**, *141*, 15605-15610.

(28) Shen, D.; Jin, W.; Bai, Y.; Huang, Y.; Lyu, H.; Zeng, L.; Wang, M.; Tang, Y.; Wan, W.; Dong, X.; Gao, Z.; Piao, H.-L.; Liu, X.; Liu, Y. Rational Design of Crystallization-Induced-Emission Probes to Detect Amorphous Protein Aggregation in Live Cells. *Angew. Chem. Int. Ed.* **2021**, *60*, 16067-16076.

(29) Ladiwala, A. R. A.; Dordick, J. S.; Tessier, P. M. Aromatic Small Molecules Remodel Toxic Soluble Oligomers of Amyloid B through Three Independent Pathways. *J. Biol. Chem.* **2011**, *286*, 3209-3218.

(30) Mamikonyan, G.; Necula, M.; Mkrtichyan, M.; Ghochikyan, A.; Petrushina, I.; Movsesyan, N.; Mina, E.; Kiyatkin, A.; Glabe, C. G.; Cribbs, D. H.; Agadjanyan, M. G. Anti-Aβ1–11 Antibody Binds to Different B-Amyloid Species, Inhibits Fibril Formation, and Disaggregates Preformed Fibrils but Not the Most Toxic Oligomers. *J. Biol. Chem* **2007**, *282*, 22376-22386.

(31) Pul, R.; Dodel, R.; Stangel, M. Antibody-Based Therapy in Alzheimer's Disease. *Expert Opin. Biol. Ther.* **2011**, *11*, 343-357.

(32) Janus, C.; Pearson, J.; McLaurin, J.; Mathews, P. M.; Jiang, Y.; Schmidt, S. D.; Chishti, M. A.; Horne, P.; Heslin, D.; French, J.; Mount, H. T. J.; Nixon, R. A.; Mercken, M.; Bergeron, C.; Fraser, P. E.; St George-Hyslop, P.; Westaway, D. Aβ Peptide Immunization Reduces Behavioural Impairment and Plaques in a Model of Alzheimer's Disease. *Nature* **2000**, *408*, 979-982.

(33) McLaurin, J.; Cecal, R.; Kierstead, M. E.; Tian, X.; Phinney, A. L.; Manea, M.; French, J. E.; Lambermon, M. H. L.; Darabie, A. A.; Brown, M. E.; Janus, C.; Chishti, M. A.; Horne, P.; Westaway, D.; Fraser, P. E.; Mount, H. T. J.; Przybylski, M.; St George-Hyslop, P. Therapeutically Effective Antibodies against Amyloid-B Peptide Target Amyloid-B Residues 4–10 and Inhibit Cytotoxicity and Fibrillogenesis. *Nature Medicine* **2002**, *8*, 1263-1269.

(34) Legleiter, J.; Czilli, D. L.; Gitter, B.; DeMattos, R. B.; Holtzman, D. M.; Kowalewski, T. Effect of Different Anti-Aβ Antibodies on Aβ Fibrillogenesis as Assessed by Atomic Force Microscopy. *J. Mol. Biol.* **2004**, *335*, 997-1006.

(35) Wulff, G. Enzyme-Like Catalysis by Molecularly Imprinted Polymers. *Chem. Rev.* **2002**, *102*, 1-28.

(36) Haupt, K.; Mosbach, K. Molecularly Imprinted Polymers and Their Use in Biomimetic Sensors. *Chem. Rev.* **2000**, *100*, 2495-2504.

(37) Ye, L.; Mosbach, K. Molecular Imprinting: Synthetic Materials as Substitutes for Biological Antibodies and Receptors. *Chem. Mater.* **2008**, *20*, 859-868.

(38) Rachkov, A.; Minoura, N. Towards Molecularly Imprinted Polymers Selective to Peptides and Proteins. The Epitope Approach. *Biochim. Biophys. Acta, Protein Struct. Mol. Enzymol.* **2001**, *1544*, 255-266.

(39) Hoshino, Y.; Kodama, T.; Okahata, Y.; Shea, K. J. Peptide Imprinted Polymer Nanoparticles: A Plastic Antibody. *J. Am. Chem. Soc.* **2008**, *130*, 15242-15243.

(40) Zeng, Z.; Hoshino, Y.; Rodriguez, A.; Yoo, H.; Shea, K. J. Synthetic Polymer Nanoparticles with Antibody-Like Affinity for a Hydrophilic Peptide. *ACS Nano* **2010**, *4*, 199-204.

(41) Urraca, J. L.; Aureliano, C. S. A.; Schillinger, E.; Esselmann, H.; Wiltfang, J.; Sellergren, B. Polymeric Complements to the Alzheimer's Disease Biomarker B-Amyloid Isoforms Aβ1–40 and Aβ1–42 for Blood Serum Analysis under Denaturing Conditions. *J. Am. Chem. Soc.* **2011**, *133*, 9220-9223.

(42) Bossi, A. M.; Sharma, P. S.; Montana, L.; Zoccatelli, G.; Laub, O.; Levi, R. Fingerprint-Imprinted Polymer: Rational Selection of Peptide Epitope Templates for the Determination of Proteins by Molecularly Imprinted Polymers. *Anal. Chem.* **2012**, *84*, 4036-4041.

(43) Yang, K.; Liu, J.; Li, S.; Li, Q.; Wu, Q.; Zhou, Y.; Zhao, Q.; Deng, N.; Liang, Z.; Zhang, L.; Zhang, Y. Epitope Imprinted Polyethersulfone Beads by Self-Assembly for Target Protein Capture from the Plasma Proteome. *Chemical Communications* **2014**, *50*, 9521-9524.

(44) Zhang, Y.; Deng, C.; Liu, S.; Wu, J.; Chen, Z.; Li, C.; Lu, W. Active Targeting of Tumors through Conformational Epitope Imprinting. *Angew. Chem. Int. Ed.* **2015**, *54*, 5157-5160.

(45) Li, S.; Yang, K.; Deng, N.; Min, Y.; Liu, L.; Zhang, L.; Zhang, Y. Thermoresponsive Epitope Surface-Imprinted Nanoparticles for Specific Capture and Release of Target Protein from Human Plasma. *ACS Appl. Mater. Interfaces* **2016**, *8*, 5747-5751.

(46) Schwark, S.; Sun, W.; Stute, J.; Lutkemeyer, D.; Ulbricht, M.; Sellergren, B. Monoclonal Antibody Capture from Cell Culture Supernatants Using Epitope Imprinted Macroporous Membranes. *RSC Adv.* **2016**, *6*, 53162-53169.

(47) Cecchini, A.; Raffa, V.; Canfarotta, F.; Signore, G.; Piletsky, S.; MacDonald, M. P.; Cuschieri, A. In Vivo Recognition of Human Vascular Endothelial Growth Factor by Molecularly Imprinted Polymers. *Nano Lett.* **2017**, *17*, 2307-2312.

(48) Pan, G.; Shinde, S.; Yeung, S. Y.; Jakštaitė, M.; Li, Q.; Wingren, A. G.; Sellergren, B. An Epitope‐Imprinted Biointerface with Dynamic Bioactivity for Modulating Cell–Biomaterial Interactions. *Angew. Chem. Int. Ed.* **2017**, *56*, 15959-15963.

(49) Qin, Y.-P.; Jia, C.; He, X.-W.; Li, W.-Y.; Zhang, Y.-K. Thermosensitive Metal Chelation Dual-Template Epitope Imprinting Polymer Using Distillation–Precipitation Polymerization for Simultaneous Recognition of Human Serum Albumin and Transferrin. *ACS Appl. Mater. Interfaces* **2018**, *10*, 9060-9068.

(50) Xing, R.; Ma, Y.; Wang, Y.; Wen, Y.; Liu, Z. Specific Recognition of Proteins and Peptides Via Controllable Oriented Surface Imprinting of Boronate Affinity-Anchored Epitopes. *Chem. Sci.* **2019**, *10*, 1831-1835.

(51) Li, X.; Palhano Zanela, T. M.; Underbakke, E. S.; Zhao, Y. Controlling Kinase Activities by Selective Inhibition of Peptide Substrates. *J. Am. Chem. Soc.* **2021**, *143*, 639-643.

(52) Li, X.; Chen, K.; Zhao, Y. Sequence-Selective Protection of Peptides from Proteolysis. *Angew. Chem. Int. Ed.* **2021**, *60*, 11092-11097.

(53) Awino, J. K.; Zhao, Y. Protein-Mimetic, Molecularly Imprinted Nanoparticles for Selective Binding of Bile Salt Derivatives in Water. *J. Am. Chem. Soc.* **2013**, *135*, 12552-12555.

(54) Zimmerman, S. C.; Wendland, M. S.; Rakow, N. A.; Zharov, I.; Suslick, K. S. Synthetic Hosts by Monomolecular Imprinting inside Dendrimers. *Nature* **2002**, *418*, 399-403.

(55) Zimmerman, S. C.; Lemcoff, N. G. Synthetic Hosts Via Molecular Imprinting-Are Universal Synthetic Antibodies Realistically Possible? *Chem. Commun.* **2004**, 5-14.

(56) Awino, J. K.; Gunasekara, R. W.; Zhao, Y. Sequence-Selective Binding of Oligopeptides in Water through Hydrophobic Coding. *J. Am. Chem. Soc.* **2017**, *139*, 2188-2191.

(57) Fa, S.; Zhao, Y. Water-Soluble Nanoparticle Receptors Supramolecularly Coded for Acidic Peptides. *Chem. -Eur. J.* **2018**, *24*, 150-158.

(58) Fa, S.; Zhao, Y. Peptide-Binding Nanoparticle Materials with Tailored Recognition Sites for Basic Peptides. *Chem. Mater.* **2017**, *29*, 9284-9291.

(59) Fa, S.; Zhao, Y. General Method for Peptide Recognition in Water through Bioinspired Complementarity. *Chem. Mater.* **2019**, *31*, 4889-4896.

(60) Zangiabadi, M.; Zhao, Y. Molecularly Imprinted Polymeric Receptors with Interfacial Hydrogen Bonds for Peptide Recognition in Water. *ACS Appl. Polym. Mater.* **2020**, *2*, 3171-3180.

(61) Zangiabadi, M.; Zhao, Y. Selective Binding of Complex Glycans and Glycoproteins in Water by Molecularly Imprinted Nanoparticles. *Nano Lett.* **2020**, *20*, 5106-5110.

(62) Petkova, A. T.; Yau, W.-M.; Tycko, R. Experimental Constraints on Quaternary Structure in Alzheimer's B-Amyloid Fibrils. *Biochemistry* **2006**, *45*, 498-512.

(63) Biancalana, M.; Koide, S. Molecular Mechanism of Thioflavin-T Binding to Amyloid Fibrils. *Biochim. Biophys. Acta* **2010**, *1804*, 1405-1412.

(64) Enache, T. A.; Chiorcea-Paquim, A.-M.; Oliveira-Brett, A. M. Amyloid Beta Peptide Vhhq, Klvff, and Iiglmvggvv Domains Involved in Fibrilization: Afm and Electrochemical Characterization. *Anal. Chem.* **2018**, *90*, 2285-2292.

(65) Greenfield, N. J. Using Circular Dichroism Spectra to Estimate Protein Secondary Structure. *Nat. Protoc.* **2006**, *1*, 2876-2890.

(66) Barrow, C. J.; Zagorski, M. G. Solution Structures of B Peptide and Its Constituent Fragments: Relation to Amyloid Deposition. *Science* **1991**, *253*, 179-182.

(67) Low, K. J. Y.; Venkatraman, A.; Mehta, J. S.; Pervushin, K. Molecular Mechanisms of Amyloid Disaggregation. *J. Adv. Res.* **2022**, *36*, 113-132.

(68) Goloubinoff, P.; Rios, P. D. L. The Mechanism of Hsp70 Chaperones: (Entropic) Pulling the Models Together. *Trends Biochem. Sci.* **2007**, *32*, 372-380.

(69) Gunasekara, R. W.; Zhao, Y. A General Method for Selective Recognition of Monosaccharides and Oligosaccharides in Water. *J. Am. Chem. Soc.* **2017**, *139*, 829-835.

(70) Salvagnini, C.; Gharbi, S.; Boxus, T.; Marchand-Brynaert, J. Synthesis and Evaluation of a Small Library of Graftable Thrombin Inhibitors Derived from (L)-Arginine. *Eur. J. Med. Chem.* **2007**, *42*, 37-53.